Reactive Sputtering of ZrN Thin Films Toward Superconducting Qubit Materials

Senuri Rupasinghe
Quantum Science and Technology, MS
Columbia University
New York, NY, 10027

Anthony Bollinger, PhD
Department of Condensed Matter Physics
Brookhaven National Laboratory
Upton, NY, 11973

Abhay Narayan Pasupathy, PhD
Department of Condensed Matter Physics
Brookhaven National Laboratory
Upton, NY, 11973

***Abstract*—Zirconium nitride (ZrN) is a promising alternative superconducting material for quantum devices because of its CMOS-compatible fabrication, chemically stable surface, and reported superconducting transition temperatures of several kelvin in thin films. In this work, a custom DC magnetron reactive sputtering system was designed, commissioned, and used to grow ZrN thin films from an elemental Zr target on Si and MgO substrates. Growth conditions were systematically varied through Ar:N_2 flow ratio, working pressure, substrate temperature, substrate material, and cooldown environment. Four-terminal resistance measurements from approximately 300 K to 3–4 K revealed transport ranging from strongly nonmetallic to metallic, demonstrating a strong dependence of film properties on deposition conditions. Elevated substrate temperature alone did not consistently improve transport on Si; however, metallic behavior was recovered when the cooldown environment was changed from vacuum to N_2, indicating that post-deposition conditions can strongly influence heated films. Metallic transport was also obtained on MgO over a range of substrate temperatures. The strongest normal-state transport was observed for a ZrN film grown on MgO at 800 °C, which exhibited a residual-resistance ratio of $RRR = 1.293$, the largest obtained in the deposition series. Despite this improvement, no film exhibited an unambiguous four-terminal superconducting transition above the experimental base temperature. These results establish an elemental-target reactive-sputtering route capable of producing metallic ZrN and identify substrate, thermal history, and post-deposition environment as important parameters for further optimization toward superconducting films. Structural and compositional characterization will be necessary to determine whether residual disorder, nonideal stoichiometry, or impurity incorporation presently limits the superconducting state.**

***Index Terms*—zirconium nitride, ZrN, reactive sputtering, superconducting thin films, quantum materials, electrical transport**

I. Introduction

Transmon qubits are the leading hardware platform for superconducting quantum computing, but coherence times remain limited well below what materials-intrinsic loss mechanisms would in principle allow. Two-level system (TLS) defects — believed to arise from tunneling atoms or electrons in disordered, amorphous regions of a device — are widely regarded as the dominant source of this residual decoherence [1]–[3]. TLS defects concentrate at material interfaces and surfaces, including the native oxide layers that form on most superconducting films upon exposure to atmosphere [2], [3]. This has motivated a search for base-layer materials combining good superconducting properties with chemically stable, low-defect-density surfaces. Titanium nitride (TiN) coplanar waveguide resonators have demonstrated internal quality factors exceeding 10^6–10^7 [4], and TiN-on-sapphire devices have reached qubit lifetimes approaching 300 μs [5]. More recently, α-tantalum films have yielded transmon coherence times exceeding 0.3 ms, attributed largely to the low-loss native oxide Ta_2O_5 [6]. These results show that base-layer material choice, and native oxide chemistry in particular, is a first-order lever on qubit performance.

Like TiN and TaN, ZrN is a rock-salt-structured transition-metal nitride compatible with standard CMOS sputtering, and 300 mm-wafer-scale studies report a mean oxygen contamination of approximately 4 at.% in reactively sputtered ZrN films [10]. Bulk ZrN superconducts near 10 K with an upper critical field of order 6.4 T [7], and thin-film studies have recovered transitions in the 5–7.3 K range depending on growth technique, substrate, and thickness [7]–[10]. However, ZrN thin-film transport and superconducting properties are highly sensitive to stoichiometry and disorder, and bulk-like behavior is not guaranteed in sputtered films early in process development. Reliable, reproducible ZrN thin-film production is therefore a necessary prerequisite to evaluating the material as a qubit base layer. The focus of this work is therefore to determine under what growth conditions DC-sputtered ZrN approaches a superconducting transition and how those conditions affect film quality.

A key methodological choice here is *reactive* sputtering: rather than sputtering directly from a pre-formed, stoichiometric ZrN target, films are grown by sputtering an elemental (bare) zirconium target in an Ar/N_2 gas mixture, with the nitride phase forming *in situ*. Stoichiometric ZrN targets are substantially more expensive and, from the vendors surveyed for this project, carry lead times of many months — a poor fit for iterative process development. Reactive sputtering sidesteps this at the cost of moving stoichiometry control into the growth parameters themselves (Ar:N_2 ratio, pressure, substrate temperature). This matters beyond convenience: demonstrating superconductivity through this route would show that superconducting ZrN can be produced without a pre-formed nitride target, providing a more accessible path for

Brookhaven National Laboratory, and the Co-Design Center for Quantum Advantage (C2QA)

iterative materials development even if the resulting T_c does not initially match that of optimized films.

II. Experimental Methods

A. Sputtering Deposition System

All films were grown in a custom-built DC magnetron reactive sputtering system, designed, assembled, and commissioned as part of this project at the OASIS group / C2QA facility at Brookhaven National Laboratory (Fig. 1). The system is comprised of **four subsystems**: (i) a **vacuum** subsystem (Pfeiffer turbomolecular/roughing pump stack, ion gauge, convectron gauge, and a residual gas analyzer for background gas composition); (ii) a **deposition and plasma** subsystem, built around a Torus MK3 magnetron sputtering gun loaded with an elemental zirconium target, with a linear feedthrough shutter controlling target-to-substrate line of sight; (iii) a **gas delivery** subsystem, using mass flow controllers to independently meter argon and nitrogen; and (iv) a **thermal management** subsystem, comprising a substrate heater/holder plate and a recirculating water chiller. Film thickness and deposition rate were monitored *in situ* via a quartz crystal microbalance (QCM, Inficon IC6).

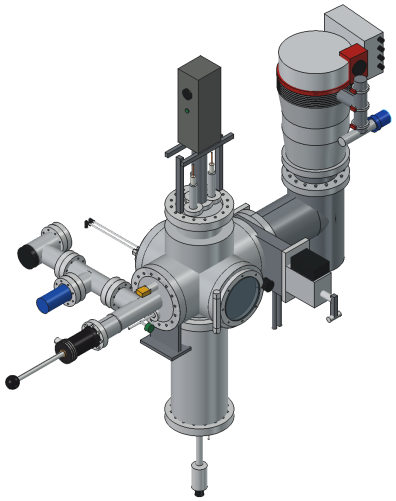

Fig. 1. CAD model of the sputtering deposition system, composed of vacuum, deposition and plasma, gas delivery, and thermal management subsystems.

B. Substrate Preparation

Si substrates were cleaned prior to loading using a 3-min acetone bath with 1 min of ultrasonication, followed by an isopropanol rinse and drying under compressed air. MgO substrates were cleaned using the same procedure with isopropanol only.

C. Sputtering Deposition

Prior to each deposition, the Zr target was pre-sputtered in Ar for approximately 15 min. The DC power was initially set to 50 W and ramped to 100 W during the final 5 min of the pre-sputter while the substrate remained isolated by the closed shutter. The deposition rate was monitored by QCM as an indicator of target poisoning (target rate $\sim$0.75 Å/s). Nitrogen was then introduced, the Ar:N_2 flow ratio and working pressure were set to the desired values, and the shutter was opened to initiate deposition. Film thickness was monitored by QCM until the target thickness was reached, at which point the power supply and gas flows were shut off and the chamber was cooled before venting. A stable reactive plasma, characteristic of steady-state deposition, is shown in Fig. 2. Substrate heating, where used, was applied throughout deposition via the substrate heater/holder plate; the cooldown atmosphere (vacuum vs. flowing N_2) was varied as described in Section II-D.

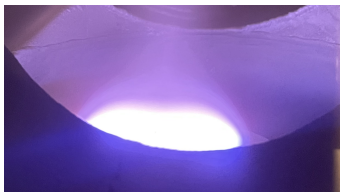

Fig. 2. Reactive DC magnetron plasma during steady-state ZrN deposition, viewed through the chamber viewport.

Over the course of this study, 17 ZrN thin-film deposition runs were performed. Table I summarizes the substrate used, working pressure, Ar:N_2 ratio, substrate heating, and deposition rate for every thin film produced. Note that power (100 W), target-to-substrate distance (5.5 in), and base pressure ($\sim 1 \times 10^{-7}$ Torr) were held fixed throughout.

D. Substrate Heating

In the latter portion of the study, substrate temperature was introduced as an additional growth parameter, motivated by the expectation that increased adatom mobility at elevated temperature could improve film crystallinity. Substrate temperatures from 300 to 800 °C were investigated. For most heated depositions, growth began after the substrate reached the target temperature. For Run 17, the MgO substrate was instead held at 800 °C for 1 h prior to deposition. The cooldown environment was also varied between vacuum and flowing N_2 to investigate the influence of post-deposition thermal history on transport.

E. QCM Tooling Factor Correction

At the start of this study, QCM reported thickness was used to standardize target thickness across films. To acquire a more accurate film thickness reading, Run 11 (QCM-reported thickness 12.0 nm) was measured in tapping-mode AFM across a lithographically defined step edge. Eight independent horizontal line profiles were extracted across the step (Fig. 3); for each, the film and substrate plateaus were separated by two-component clustering of the height values, and step height computed as the difference between plateau means (Fig. 4). Step heights ranged 13.1–19.9 nm across the eight profiles, giving a mean thickness of 16.2. This measurement gives an estimated tooling correction factor of $16.2/12.0 = 1.35$. This factor was applied to the nominal QCM thicknesses reported

TABLE I
THIN-FILM DEPOSITION PARAMETERS FOR RUNS 1–17.

Run	Substrate	Thickness (Å)	Power (W)	Pressure (mTorr)	Ar:N_2 Flows (sccm)	Substrate Temp. (°C)	Rate (Å/s)
1	Si	675	100	3	18.0:2.0	20	0.75
2	Si	675	100	4	42:1	20	1.14
3	Si	675	100	5	68.7:1	20	1.34
4	Si	675	100	5	30:1	20	1.01
5	Si	675	100	5	20:1	20	0.90
6	Si	675	100	5	20:1	20	0.95
7	Si	675	100	5	30:1	20	1.14
8	Si	675	100	5	30:1	20	1.07
9	Si	675	100	5	10:1	20	0.95
10	Si	675	100	5	30:1	300	1.05
11	Si	162	100	5	30:1	20	1.10
12	Si	675	100	5	30:1	500	1.02
13	Si	675	100	5	30:1	500	0.93
14	MgO	675	100	5	30:1	20	1.05
15	MgO	675	100	5	30:1	500	1.07
16	Si	675	100	5	30:1	500	1.06
17	MgO	1105	100	5	30:1	800*	1.44

*For Run 17, the MgO substrate was held at 800 °C for 1 h prior to deposition.

in Table I; consequently, the tabulated thicknesses should be regarded as corrected estimates rather than independent thickness measurements of each film.

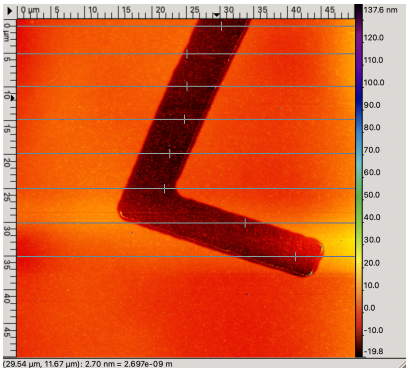

Fig. 3. Eight horizontal profiles were used to calculate the tooling factor of this sputtering deposition system.

F. Measurement

Films were wire-bonded in a four-terminal (Kelvin) configuration for electrical transport measurements (Fig. 5), with four wire bonds per side arranged collinearly with approximately 2 mm spacing. The four-terminal configuration separates the voltage-sensing leads from the current-carrying leads, thereby minimizing contributions from contact and lead resistances to the measured film resistance. Samples were mounted in a cryostat and cooled from room temperature to cryogenic temperatures, with resistance recorded continuously as a function of temperature, $R(T)$, during cooling and warming sweeps. A current bias of 10 μA with alternating polarity was applied through the outer current contacts, while the voltage across the inner voltage contacts was measured independently. The four-terminal resistance was calculated as $R = V/I$. A two-probe voltage and corresponding two-probe resistance were recorded simultaneously for diagnostic purposes; the four-terminal resistance was used for the $R(T)$ analysis.

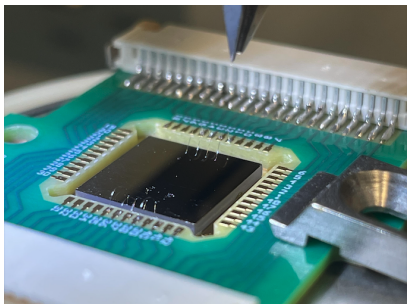

Fig. 5. Eight wire bond contacts on ZrN thin film prior to measurement.

III. RESULTS

A. Temperature-Dependent Electrical Transport

The temperature-dependent electrical resistance of the ZrN thin films was measured from approximately 300 K to 3–4 K. The deposition conditions for Runs 1–17 are summarized in Table I. Because the absolute measured resistance depends on both the intrinsic film resistivity and the sample geometry, the resistance curves were normalized to their room-temperature values according to

$$R_{\mathrm{norm}}(T) = \frac{R(T)}{R(300\,\mathrm{K})}. \tag{1}$$

Figure 6 shows the normalized $R(T)$ characteristics obtained from the usable four-terminal R_{ch1} measurements. To quantify the temperature dependence, the residual-resistance ratio (RRR) was defined as

$$RRR = \frac{R(300\,\mathrm{K})}{R(4\,\mathrm{K})}, \tag{2}$$

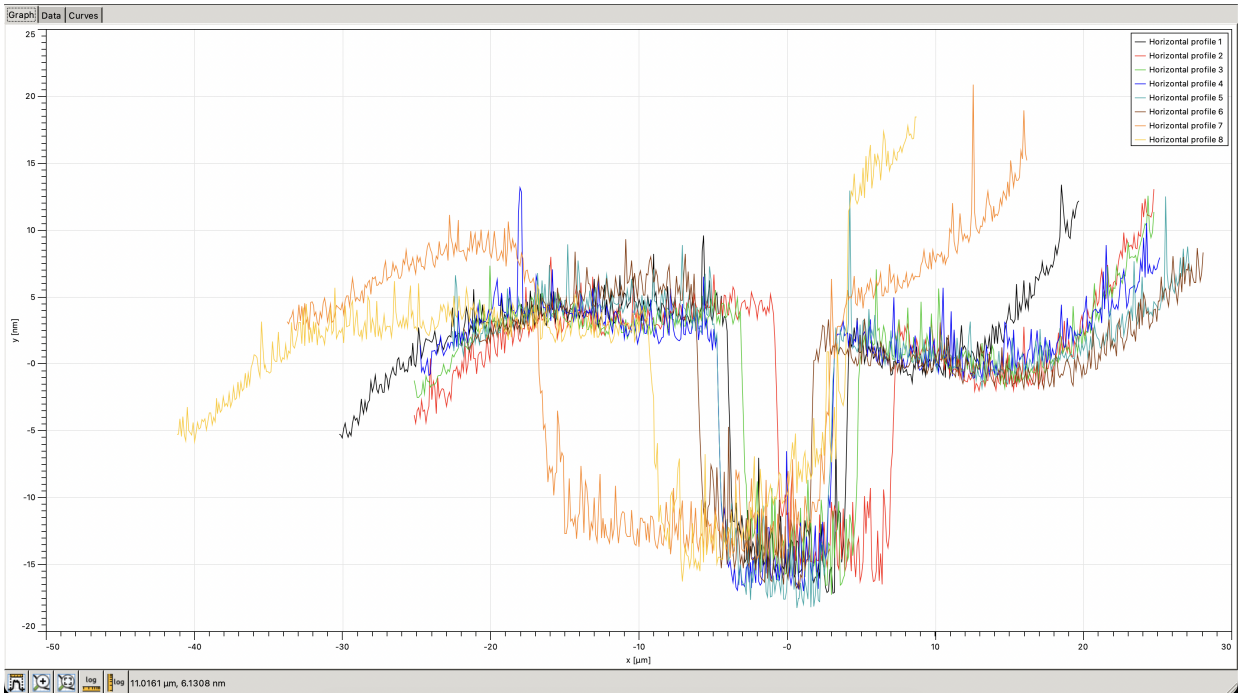

Fig. 4. Film and substrate plateaus were separated by two-component clustering of the height values, and step height computed as the difference between plateau means.

where the nearest measured temperature was used when a data point was not available at exactly 300 K or 4 K. Thus, $RRR > 1$ corresponds to predominantly metallic behavior, whereas $RRR < 1$ indicates an increase in resistance upon cooling. Measurements that did not span a sufficient temperature range or exhibited clear measurement artifacts were excluded from the RRR analysis.

As shown in Fig. 6, the deposition series produced a broad range of temperature-dependent transport behavior. Many films exhibited metallic conduction, characterized by decreasing resistance with decreasing temperature, although the magnitude of the temperature dependence varied substantially between runs. Other measurements exhibited weakly or strongly nonmetallic behavior. The corresponding RRR values are summarized in Table II.

In addition to the normalized resistance curves, the measured $R_{\mathrm{ch1}}(T)$ characteristics are summarized by run in Fig. 7. Presenting the measurements on their absolute resistance scales highlights substantial variation in both resistance magnitude and temperature dependence across the deposition series.

Figure 7 illustrates that the transport characteristics do not evolve monotonically with run number. Rather, substantial changes in both the absolute resistance and the shape of $R(T)$ occur as the deposition conditions are varied. Differences between measurements obtained from the same film further indicate spatial and/or measurement-geometry-dependent variation in portions of the deposition series.

The early deposition series demonstrates that metallic transport could be obtained under several room-temperature growth conditions. Run 2 exhibited RRR values of approximately 1.08–1.09, while measurements from Run 4 reached approximately 1.15–1.17. One region of Run 8 exhibited an RRR of approximately 1.19, among the largest values obtained in the room-temperature Si series. In contrast, Run 9 exhibited strongly nonmetallic transport. Its usable warming measurement yielded $RRR \approx 0.49$, corresponding to an approximately twofold increase in normalized resistance between room temperature and the lowest measured temperatures.

TABLE II
RESIDUAL-RESISTANCE RATIOS OBTAINED FROM USABLE $R_{\mathrm{ch1}}(T)$ MEASUREMENTS SPANNING APPROXIMATELY 300 K TO 4 K. RRR WAS CALCULATED USING THE NEAREST MEASURED TEMPERATURES WHEN DATA WERE NOT ACQUIRED AT EXACTLY 300 K AND 4 K.

Run	Measurement	RRR
2	Less Gold	1.082
2	More Gold	1.089
3	Less Gold-1	1.062
4	Side 1	1.165
4	Side 2	1.147
6	Side 1	1.016
8	Region A	1.192
9	Warming	0.486
10	Cooling	0.944
12	Cooling	0.859
12	Warming	0.944
13	Cooling	1.133
13	Warming	1.047
14	Cooling	1.073
14	Warming	1.080
15	Cooling	1.084
16	Warming	1.065
17	Cooling	**1.293**

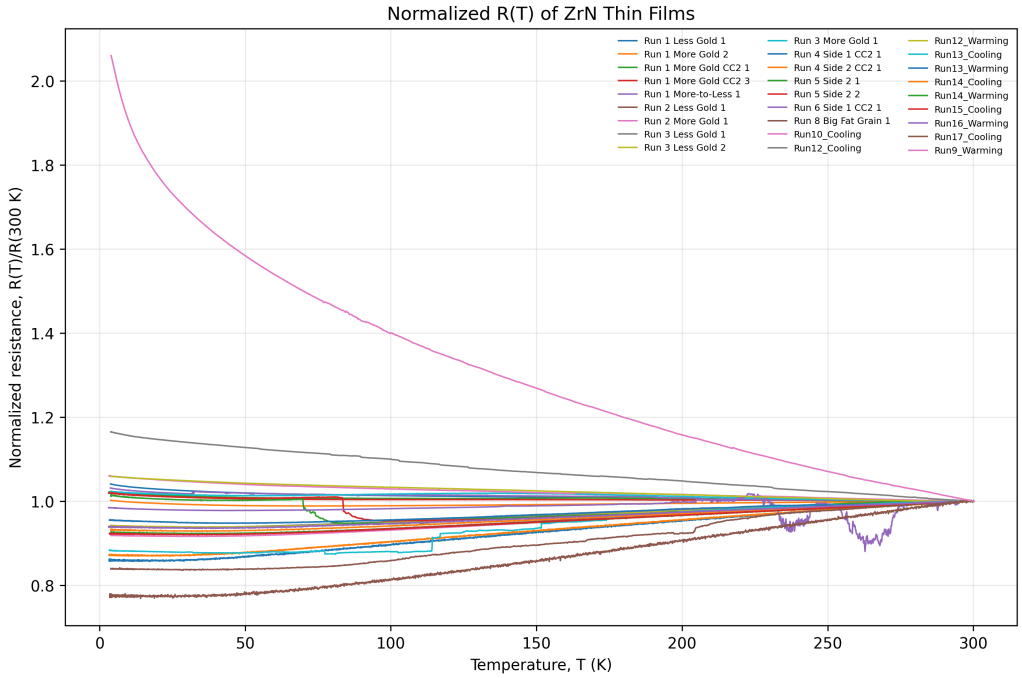

Fig. 6. Normalized temperature-dependent resistance $R(T)/R(300\,\mathrm{K})$ for usable ZrN thin-film measurements from Runs 1–17. The films exhibit transport ranging from nonmetallic to metallic behavior. No zero-resistance superconducting transition was observed within the measured temperature range.

B. Substrate Heating Study

The effect of substrate heating was first investigated using Si substrates. Relative to the metallic behavior obtained for selected room-temperature-grown films, elevated-temperature growth did not initially produce improved electrical transport. Run 10, deposited at 300 °C, exhibited weakly nonmetallic behavior, while Run 12, deposited at 500 °C, showed a substantially stronger resistance increase upon cooling. Run 12 had a resistance of approximately $555\ \Omega$ at 300 K and increased further at low temperature, yielding $RRR < 1$ (Table II).

A significant change was observed for Run 13, which was also deposited on Si at 500 °C but was cooled under N_2 rather than under vacuum. Run 13 exhibited metallic transport, with the resistance decreasing from approximately $76\ \Omega$ at room temperature to approximately $69\ \Omega$ at low temperature. The cooling measurement yielded $RRR \approx 1.13$, in contrast to the nonmetallic behavior of Run 12. The recovery of metallic transport when the cooldown atmosphere was changed indicates that the post-deposition environment is an important experimental parameter for heated ZrN films.

Two small discontinuities are visible in the Run 13 $R(T)$ trace near approximately 75 K and 115 K [Fig. 7]. Related features are present in both the two-terminal and four-terminal signals, making an artifact confined solely to the four-terminal voltage contacts unlikely. Their origin was not determined, but they do not alter the overall metallic temperature dependence of Run 13.

Run 16, also deposited on Si at 500 °C, exhibited metallic behavior over most of the measured temperature range. Its resistance decreased from approximately $4.26\ \Omega$ at 300 K to approximately $4.00\ \Omega$ near 4 K, corresponding to

$$RRR_{16} \approx 1.065. \tag{3}$$

A shallow resistance minimum occurred near 40 K, followed by a small low-temperature upturn. Taken together, the heated Si measurements show that substrate temperature alone does not determine the resulting transport and that post-deposition conditions can substantially affect the measured behavior.

C. MgO Substrate Study

The influence of substrate material was further investigated using MgO. Three films were deposited on MgO using an Ar:N_2 flow ratio of 30:1: Run 14 near room temperature, Run 15 at 500 °C, and Run 17 at 800 °C.

Run 14 exhibited metallic transport without substrate heating, with the resistance decreasing from approximately $56\ \Omega$ at 300 K to approximately $50\ \Omega$ at low temperature. Cooling and warming measurements yielded $RRR \approx 1.07$–1.08 (Table II), demonstrating that metallic ZrN could be obtained on MgO using the present deposition process.

Run 15 was grown on MgO at 500 °C and also exhibited metallic transport. Its resistance decreased from approximately $101\ \Omega$ at room temperature to approximately $93\ \Omega$ at low temperature, yielding $RRR \approx 1.08$. This behavior contrasts with the nonmetallic transport observed for Run 12, which was grown on Si at the same nominal substrate temperature. Because these comparisons are based on individual deposition runs, the respective effects of substrate material, cooldown

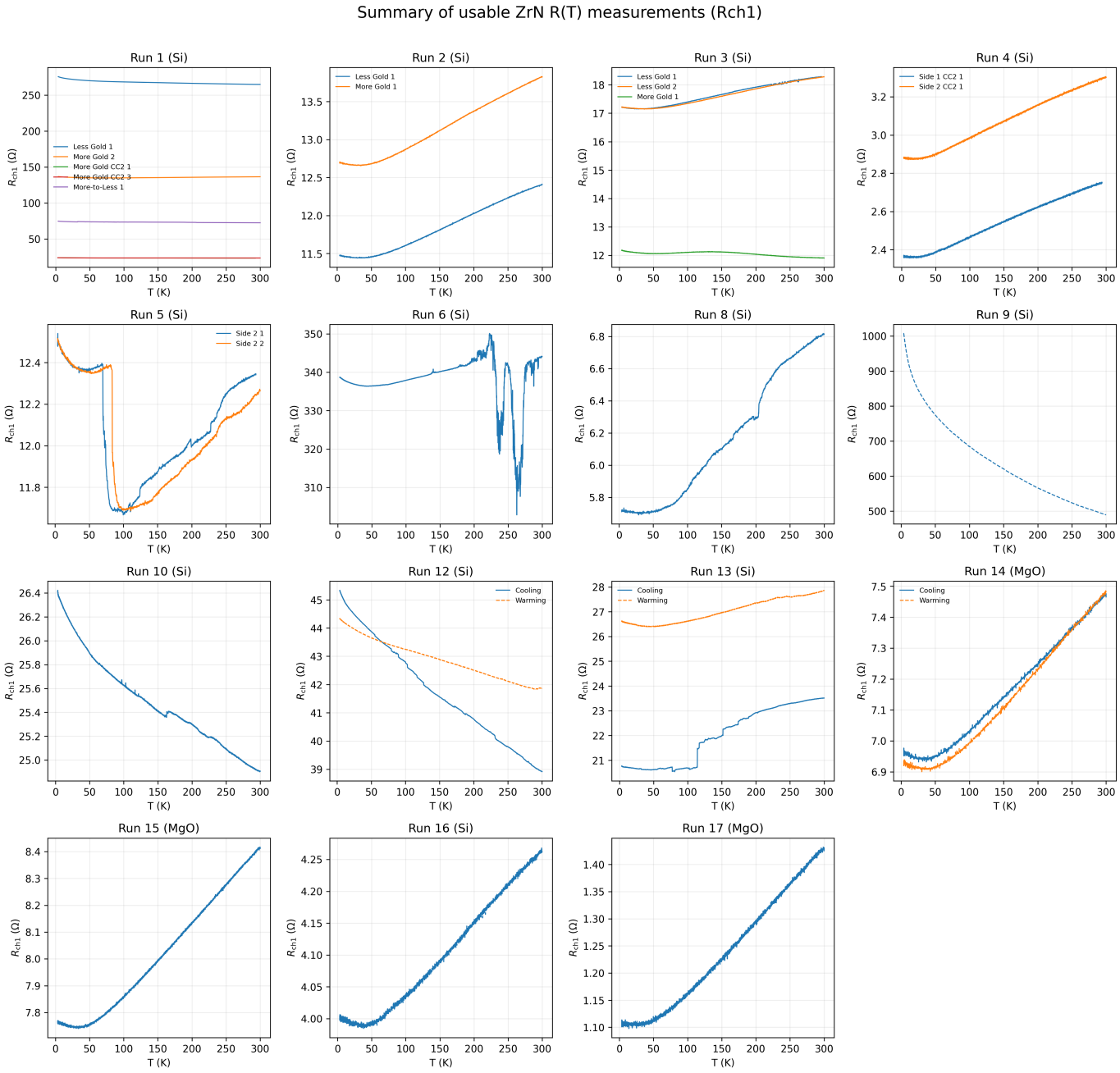

Fig. 7. Summary of the usable four-terminal $R_{\mathrm{ch1}}(T)$ measurements for the ZrN thin-film deposition series. Each panel displays the measured resistance on its absolute scale. Multiple traces are shown where measurements were obtained from different sample regions, contact configurations, or thermal sweeps; traces identified as clear measurement artifacts were excluded from quantitative comparisons. Metallic, weakly temperature-dependent, and nonmetallic transport are observed across the deposition series.

environment, and run-to-run variation cannot be uniquely separated.

The strongest metallic transport of the deposition series was obtained for Run 17, grown on MgO at 800 °C. Figure 8 compares the normalized resistance of Runs 14–17.

For Run 17, the four-terminal resistance decreased from approximately $1.428\ \Omega$ at 300 K to $1.105\ \Omega$ near 4 K, corresponding to

$$RRR_{17} \approx 1.293. \tag{4}$$

This represents the largest RRR obtained among the measured films. A shallow resistance minimum of approximately $1.098\ \Omega$ occurred near 14 K, below which only a small resistance upturn was observed. No transition to a zero-resistance state occurred above the minimum measurement temperature.

The MgO measurements therefore show metallic transport over the investigated substrate-temperature range, with Run 17 exhibiting the strongest normal-state temperature dependence. Run 17 also differed from Runs 14 and 15 in film thickness and thermal history, so the improvement cannot be assigned exclusively to substrate temperature.

D. Comparison of Four-Terminal and Two-Terminal Resistance

For selected measurements, the two-terminal resistance $R_{2\mathrm{p}}$ was recorded simultaneously with R_{ch1}. The four-terminal quantity R_{ch1} predominantly measures the resistance of the film region between the voltage contacts, whereas $R_{2\mathrm{p}}$ includes additional contributions from the complete current path, including contacts, interfaces, leads, and portions of the film outside the voltage contacts.

This distinction is evident in Runs 16 and 17. For Run 16, R_{ch1} was approximately $4\ \Omega$, whereas $R_{2\mathrm{p}}$ was approximately 68–73 Ω. Run 17 exhibited substantially smaller values of both quantities, with $R_{\mathrm{ch1}} \approx 1.1$–$1.4\ \Omega$ and $R_{2\mathrm{p}} \approx 30$–$35\ \Omega$. The large difference between the two measurements demonstrates that a substantial contribution to the two-terminal resistance arises outside the region directly sampled by the four-terminal voltage contacts.

A small low-temperature feature was observed in $R_{2\mathrm{p}}$ for Run 17, but no corresponding decrease occurred in R_{ch1}. The feature therefore does not correspond to a zero-resistance transition in the film region sampled by the four-terminal voltage probes.

E. Search for a Superconducting Transition

No unambiguous superconducting transition was observed in the four-terminal measurements above the minimum accessible temperature of approximately 3–4 K. None of the usable $R_{\mathrm{ch1}}(T)$ traces exhibited a sharp decrease toward zero resistance.

Several metallic films instead exhibited shallow low-temperature resistance minima followed by weak upturns. The characteristic temperature of this feature varied between samples, decreasing from approximately 40 K in Run 16 to approximately 14 K in Run 17. Run 17 nevertheless retained a finite four-terminal resistance of approximately $1.1\ \Omega$ at the lowest measured temperature despite exhibiting the largest RRR of the deposition series.

IV. Discussion

The transport measurements demonstrate that achieving metallic ZrN is not by itself sufficient to obtain an observable superconducting transition. Across the deposition series, the films ranged from strongly nonmetallic to metallic, yet no four-terminal transition to a zero-resistance state was observed above approximately 3–4 K. The variation in RRR therefore provides a useful empirical measure of normal-state transport quality, while the continued absence of superconductivity indicates that additional materials limitations remain.

Several metallic films exhibited a shallow resistance minimum followed by a weak low-temperature upturn. Such behavior is commonly observed in disordered conducting thin films and can arise from quantum corrections to the conductivity, including weak-localization and electron-electron- interaction effects [11]. The present $R(T)$ measurements alone, however, cannot distinguish these mechanisms from other possible sources of the upturn. The feature is therefore treated here as evidence for an additional low-temperature transport contribution rather than being assigned to a specific microscopic mechanism.

The evolution from Run 16 to Run 17 is particularly informative. The resistance minimum shifted from approximately 40 K to approximately 14 K while the RRR increased from approximately 1.07 to 1.29. This combination is consistent with a reduced relative contribution from the mechanism responsible for the low-temperature resistance upturn in Run 17. The absolute resistance of Run 17 was also substantially smaller; however, absolute resistance must be interpreted cautiously because it depends on film thickness and lateral measurement geometry. RRR is therefore the more robust metric for comparing normal-state temperature dependence between films, since the geometrical factor cancels within a given measurement.

Published ZrN films optimized for superconducting applications exhibit superconducting transitions within the temperature range accessible to the present measurements. Potjan *et al.*, for example, reported superconducting reactively sputtered ZrN while also showing that such films can deviate substantially from ideal ZrN stoichiometry [10]. The comparatively small RRR values observed for most films in the present study indicate relatively weak temperature dependence of the resistance, even when the overall $R(T)$ behavior is metallic. Structural disorder is known to suppress superconductivity in ZrN; ion-irradiation measurements on stoichiometric ZrN films showed a continuous reduction of T_c from approximately 9.2 K to 3.8 K with increasing disorder [12]. Thus, obtaining a positive metallic temperature coefficient should be regarded as an intermediate step rather than evidence that the film has reached the materials quality required for superconductivity. Notably, the demonstrated suppression of T_c into the few-kelvin range makes a superconducting transition below the

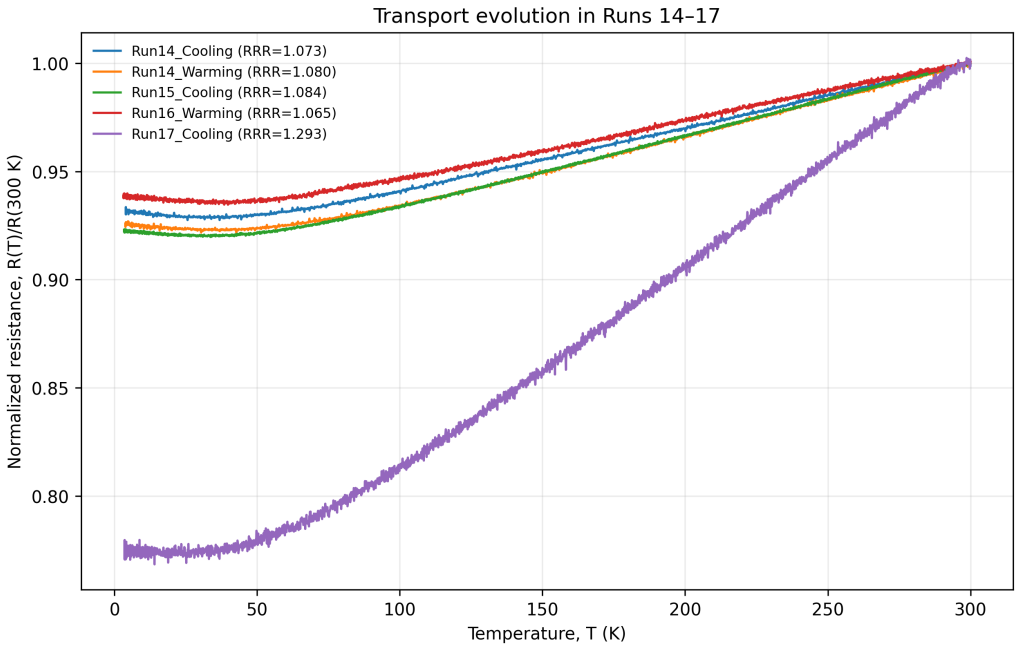

Fig. 8. Normalized temperature-dependent resistance for Runs 14–17. Run 17 exhibits the strongest temperature dependence and the largest residual-resistance ratio, $RRR = 1.293$.

present measurement floor physically plausible, although the present measurements provide no evidence that such a transition occurs.

The substrate-heating study further demonstrates the sensitivity of ZrN transport to both growth and post-growth conditions. Heating Si substrates did not produce a monotonic improvement: Runs 10 and 12 exhibited nonmetallic behavior despite elevated growth temperatures, whereas Run 13, grown on Si at 500 °C and cooled under N_2, recovered metallic transport. The contrast between Runs 12 and 13 suggests that the cooldown environment can strongly influence the electrical properties of heated films.

One possible explanation is that vacuum cooldown modifies the film stoichiometry, including possible nitrogen loss, thereby increasing disorder or altering the electronic structure. The transport measurements do not directly measure composition, however, and nitrogen loss therefore cannot be established as the mechanism from the present data alone. This distinction is particularly important for reactive sputtering from an elemental Zr target, for which the nitrogen content of the deposited film is established during the reactive growth process. Deviations from ideal stoichiometry and impurity incorporation may provide additional sources of scattering and can alter superconducting properties [10], [13]. Recent work on bulk, nonstoichiometric rock-salt zirconium nitrides further found that T_c varies systematically with composition and the N/Zr ratio [13]. Potjan *et al.* reported reactively sputtered ZrN with a composition of approximately $ZrN_{0.74\pm0.02}$ together with oxygen incorporation [10]. Direct compositional measurements are therefore needed to determine whether similar effects occur in the present films.

The MgO deposition series suggests that substrate choice is another important parameter in the growth optimization. Run 14 demonstrated that metallic ZrN could be obtained on MgO without substrate heating, while Run 15 remained metallic following growth at 500 °C. The latter behavior contrasts with the poorer transport observed in heated Si films under comparable nominal temperature conditions. The substrate dependence could reflect differences in film nucleation, crystalline texture, interfacial chemistry, strain, or defect structure. The present transport measurements cannot distinguish among these possibilities and therefore motivate direct structural comparison of Si- and MgO-supported films.

Run 17 provides the strongest evidence that the explored growth conditions can substantially improve normal-state ZrN transport. Grown on MgO at 800 °C, it exhibited the largest RRR of the deposition series ($RRR = 1.293$) and the lowest-temperature resistance minimum. However, Run 17 also differed from the preceding films in thickness and thermal history. The result therefore identifies the Run 17 growth condition as the most promising region of the parameter space explored here, rather than establishing a unique causal role for either MgO or the 800 °C substrate temperature.

Despite this improvement, Run 17 did not exhibit a superconducting transition. Its four-terminal resistance remained finite at the lowest measured temperature, and the small low-temperature feature in R_{2p} was not accompanied by a corresponding decrease in R_{ch1}. The two-terminal feature therefore does not provide evidence for superconductivity in the portion of the ZrN film sampled by the four-terminal voltage probes. A superconducting transition below the present measurement floor cannot be excluded, but no pronounced precursor toward

zero resistance was observed in R_{ch1}.

Taken together, these results suggest that the principal challenge is no longer simply obtaining electrically conducting ZrN, since metallic films were produced under several deposition conditions. Rather, further progress requires identifying the composition and structural quality associated with reduced scattering and superconductivity. X-ray diffraction can determine phase, texture, and crystalline quality, while compositional measurements such as XPS or RBS can test whether improved transport correlates with a more favorable Zr:N ratio or reduced oxygen incorporation. Controlled experiments that independently vary substrate material, substrate temperature, film thickness, and cooldown environment will be necessary to separate the contributions of these parameters. Finally, transport measurements extending below 3 K are required to determine whether the most metallic films possess a superconducting transition below the present experimental limit.

V. Conclusion and Future Work

This work established a reproducible reactive-sputtering and cryogenic transport-characterization process for ZrN thin films grown from an elemental Zr target. Across the deposition series, the electrical behavior ranged from strongly nonmetallic to metallic, demonstrating the sensitivity of ZrN transport to growth conditions, substrate material, and post-deposition environment. The substrate-heating study further showed that elevated temperature alone does not guarantee improved transport: heated Si films cooled under vacuum exhibited degraded behavior, whereas a subsequent heated Si film cooled under N_2 exhibited metallic transport; metallic behavior was also retained in heated films grown on MgO.

The strongest normal-state transport was obtained for Run 17, grown on MgO at 800 °C, which exhibited the largest residual-resistance ratio of the study, $RRR = 1.293$, and a substantially reduced low-temperature resistance upturn. Nevertheless, no film exhibited an unambiguous four-terminal superconducting transition above the experimental base temperature of approximately 3–4 K. The results therefore indicate that producing metallic ZrN is achievable with the present reactive-sputtering process, but further optimization and direct characterization of composition and structural quality are required to establish the conditions necessary for superconductivity.

The most important next step is to correlate transport with direct materials characterization. XRD should be used to determine phase, texture, and crystalline quality, while XPS or RBS can quantify the Zr:N ratio and oxygen incorporation. Additional growth experiments should independently vary substrate temperature, substrate material, film thickness, and cooldown environment to separate their respective contributions to transport. Measurements extending below 3 K will also be necessary to determine whether the most metallic films possess a superconducting transition below the temperature range accessible in the present study.

Ultimately, observation of superconductivity would establish that superconducting ZrN can be synthesized by reactive sputtering from an elemental Zr target without requiring a preformed stoichiometric ZrN target. The deposition and characterization capability developed here provides a foundation for that optimization and, subsequently, for evaluating ZrN in low-loss microwave resonators and superconducting quantum devices.

Acknowledgment

This work supports C2QA's mission of enabling stable, reliable, large-scale quantum computing, and the DOE Genesis Mission, by helping identify scalable, lower-loss material candidates for next-generation qubit fabrication. This project was supported in part by the U.S. Department of Energy, Office of Science, Office of Workforce Development for Teachers and Scientists (WDTS) under the Graduate Research Internship Program (GRIP).

References

[1] C. Müller, J. H. Cole, and J. Lisenfeld, "Towards understanding two-level-systems in amorphous solids: insights from quantum circuits," *Rep. Prog. Phys.* **82**, 124501 (2019).

[2] J. M. Martinis, K. B. Cooper, R. McDermott, M. Steffen, M. Ansmann, K. D. Osborn, K. Cicak, S. Oh, D. P. Pappas, R. W. Simmonds, and C. C. Yu, "Decoherence in Josephson qubits from dielectric loss," *Phys. Rev. Lett.* **95**, 210503 (2005).

[3] J. Gao, M. Daal, A. Vayonakis, S. Kumar, J. Zmuidzinas, B. Sadoulet, B. A. Mazin, P. K. Day, and H. G. Leduc, "Experimental evidence for a surface distribution of two-level systems in superconducting lithographed microwave resonators," *Appl. Phys. Lett.* **92**, 152505 (2008).

[4] M. R. Vissers, J. Gao, D. S. Wisbey, D. A. Hite, C. C. Tsuei, A. D. Corcoles, M. Steffen, and D. P. Pappas, "Low loss superconducting titanium nitride coplanar waveguide resonators," *Appl. Phys. Lett.* **97**, 232509 (2010).

[5] H. Deng *et al.*, "Titanium Nitride Film on Sapphire Substrate with Low Dielectric Loss for Superconducting Qubits," *Phys. Rev. Applied* **19**, 024013 (2023).

[6] A. P. M. Place *et al.*, "New material platform for superconducting transmon qubits with coherence times exceeding 0.3 milliseconds," *Nat. Commun.* **12**, 1779 (2021).

[7] B. J. May, S. Regmi, A. R. Khanolkar, V. Buturlim, Z. E. Cresswell, K. D. Vallejo, K. Gofryk, and D. H. Hurley, "Molecular beam epitaxy of superconducting zirconium nitride on GaN substrates," *AIP Advances* **14**, 125327 (2024).

[8] Y. Zhu, M. Ikeda, Y. Murakami, A. Tsukazaki, T. Fukumura, and M. Kawasaki, "Low-temperature growth of highly crystalline superconducting ZrN thin film on c-GaN layer by pulsed laser deposition," *Jpn. J. Appl. Phys.* **46**, L1000 (2007).

[9] O. Saritas, F. Bolle, Y. Lin, M. Dressel, R. Potjan, M. Wislicenus, A. Reck, and M. Scheffler, "THz electrodynamics and superconducting energy scales of ZrN thin films," *Appl. Phys. Lett.* **127**, 192601 (2025).

[10] R. Potjan, M. Wislicenus, O. Ostien, R. Hoffmann, M. Lederer, A. Reck, J. Emara, L. Roy, B. Lilienthal-Uhlig, and J. Wosnitza, "300 mm CMOS-compatible superconducting HfN and ZrN thin films for quantum applications," *Appl. Phys. Lett.* **123**, 172602 (2023).

[11] G. Bergmann, "Weak localization in thin films: a time-of-flight experiment with conduction electrons," *Phys. Rep.*, vol. 107, no. 1, pp. 1–58, 1984.

[12] N. Kobayashi, H. Tanoue, and G. Linker, "Defect structure and superconducting transition temperature of ion-irradiated refractory metal carbides and nitrides," *Nucl. Instrum. Methods Phys. Res. B*, vol. 33, no. 1–4, pp. 795–798, 1988.

[13] M. Tanaka, M. Fujioka, D. H. Gregory, and K. Inumaru, "Bulk synthesis and superconductivity of rock salt-type, nitrogen-rich, zirconium-deficient nitrides, $Zr_{1-x}N$," *Chem. Mater.*, vol. 37, no. 10, pp. 3747–3756, 2025.